J|A|C|S ARTICLES

Published on Web 11/06/2009

Structural, Physicochemical, and Reactivity Properties of an All-Inorganic, Highly Active Tetraruthenium Homogeneous Catalyst for Water Oxidation

Yurii V. Geletii,[†] Claire Besson,[†,‡] Yu Hou,[†] Qiushi Yin,[†] Djamaladdin G. Musaev,[§] David Quiñonero,[§] Rui Cao,[†] Kenneth I. Hardcastle,[†] Anna Proust,[‡,⊥] Paul Kögerler,[||] and Craig L. Hill*[,†]

Department of Chemistry, Emory University, Atlanta, Georgia 30322, Institut Parisien de Chimie Moléculaire, UMR CNRS 7201, UPMC Univ Paris 06, 4 Place Jussieu, Case 42, 75252, Paris Cedex 05, France, Cherry L. Emerson Center for Scientific Computation, Emory University, Atlanta, Georgia 30322, Institut für Anorganische Chemie, RWTH Aachen University, D-52074 Aachen, Germany, and Institut Universitaire de France, 103, Boulevard Saint-Michel 75005 Paris, France

Received August 28, 2009; E-mail: chill@emory.edu

Abstract: Several key properties of the water oxidation catalyst $Rb_8K_2[\{Ru^{IV}_4O_4(OH)_2(H_2O)_4\}(\gamma\text{-}SiW_{10}O_{36})_2]$ and its mechanism of water oxidation are given. The one-electron oxidized analogue $[\{Ru^{V}Ru^{IV}_3O_6(OH_2)_4\}(\gamma\text{-}SiW_{10}O_{36})_2]^{11-}$ has been prepared and thoroughly characterized. The voltammetric rest potentials, X-ray structures, elemental analysis, magnetism, and requirement of an oxidant (O_2) indicate these two complexes contain $[Ru^{IV}_4O_6]$ and $[Ru^{V}Ru^{IV}_3O_6]$ cores, respectively. Voltammetry and potentiometric titrations establish the potentials of several couples of the catalyst in aqueous solution, and a speciation diagram (versus electrochemical potential) is calculated. The potentials depend on the nature and concentration of counterions. The catalyst exhibits four reversible couples spanning only ca. 0.5 V in the H_2O/O_2 potential region, keys to efficient water oxidation at low overpotential and consistent with DFT calculations showing very small energy differences between all adjacent frontier orbitals. The voltammetric potentials of the catalyst are evenly spaced (a Coulomb staircase), more consistent with bulk-like properties than molecular ones. Catalysis of water oxidation by $[Ru(bpy)_3]^{3+}$ has been examined in detail. There is a hyperbolic dependence of O_2 yield on catalyst concentration in accord with competing water and ligand (bpy) oxidations. O_2 yields, turnover numbers, and extensive kinetics data reveal several features and lead to a mechanism involving rapid oxidation of the catalyst in four one-electron steps followed by rate-limiting H_2O oxidation/O_2 evolution. Six spectroscopic, scattering, and chemical experiments indicate that the catalyst is stable in solution and under catalytic turnover conditions. However, it decomposes slowly in acidic aqueous solutions (pH < 1.5).

Introduction

The development of effective molecular catalysts for the sustained oxidation of water is vital to the production of solar fuels (splitting of water or reduction of CO_2 to liquid fuels). As stated by Eisenberg and Gray ("Forum on Making Oxygen"): "Understanding the fundamental factors that control this complex four-electron, four-proton reaction is one of science's grand challenges because research progress in this area is absolutely essential for the development of efficient artificial photosynthetic machines to convert sunlight into stored chemical energy on an enormous scale."[1] The ideal water oxidation catalyst (WOC) should be fast, amenable to interfacing with sensitizer materials of various kinds, and stable to oxidative, hydrolytic, and thermal degradation during turnover. Furthermore, it should exhibit several electron transfer (ET) or proton coupled electron transfer (PCET) events over a narrow potential range (redox leveling) facilitating water oxidation/oxygen evolution near the thermodynamic potential (this translates to heterogeneous WOCs that turnover rapidly without an externally applied potential).

Currently, work on both heterogeneous[2−15] and homogeneous[4,16−46] water oxidation catalysts is at a record level of activity, and these two

[†] Department of Chemistry, Emory University.
[‡] UPMC Univ Paris 06.
[§] Cherry L. Emerson Center for Scientific Computation, Emory University.
[||] RWTH Aachen University.
[⊥] Institut Universitaire de France.

(1) Eisenberg, R.; Gray, H. B. *Inorg. Chem.* **2008**, *47*, 1697–1699.
(2) Shafirovich, V. Ya; Shilov, A. E. *Kinet. Katal.* **1979**, *20*, 1156–1162.
(3) Shafirovich, V.; Ya.; Khannanov, N. K.; Strelets, V. V. *Nouv. J. Chim.* **1980**, *4*, 81–84.
(4) Ghosh, P. K.; Brunschwig, B. S.; Chou, M.; Creutz, C.; Sutin, N. *J. Am. Chem. Soc.* **1984**, *106*, 4772–4783.
(5) Ramaraj, R.; Kira, A.; Kaneko, M. *Angew. Chem., Int. Ed. Engl.* **1986**, *25*, 825–827.
(6) Ramaraj, R.; Kira, A.; Kaneko, M. *Chem. Lett.* **1987**, *16*, 261–264.
(7) Harriman, A.; Richoux, M.-C.; Christensen, P. A.; Mosseri, S.; Neta, P. *J. Chem. Soc., Faraday Trans. 1* **1987**, *83*, 3001–3014.
(8) Parmon, V. N. *Catal. Today* **2000**, *58*, 55.
(9) Elizarova, G. L.; Zhidomirov, G. M.; Parmon, V. N. *Catal. Today* **2000**, *58*, 71–78.
(10) Hammarström, L.; Sun, L.; Åkermark, B.; Styring, S. *Catal. Today* **2000**, *58*, 57–69.
(11) Hoertz, P. G.; Kim, Y.-I.; Youngblood, W. J.; Mallouk, T. E. *J. Phys. Chem. B* **2007**, *111*, 6845–6856.
(12) Kanan, M. W.; Nocera, D. G. *Science* **2008**, *321*, 1072–1075.

10.1021/ja907277b CCC: $40.75

classes of WOCs have complementary strengths and weaknesses. While some heterogeneous WOCs are susceptible to hydrolytic or anodic/photoanodic corrosion, the metal oxide/hydroxide catalysts are usually both robust and potentially amenable to inexpensive production. However, most heterogeneous WOCs are far slower in catalysis per transition metal atom than the homogeneous WOCs. Homogeneous catalysts, some modeled in part on the increasingly well understood Mn_4CaO_4 active center in Photosystem II,[47−51] can be investigated, optimized, and effectively interfaced with sensitizer systems of several kinds more readily than can heterogeneous catalysts, but they have unstable organic ligands. To date, several Ru-based homogeneous WOCs,[17−20,23,24,26,27,35−42,45,52] starting with the famous "blue dimer" of Meyer,[17,39] several Mn-based[21,22,25,29,30,32−34,46,53] and three organometallic homogeneous WOCs[31,43,44] have been reported. Immobilization of homogeneous WOCs can increase the total turnovers before inactivation,[54] and soluble redox mediators can increase the rates of immobilized WOCs.[39] A few in-depth recent mechanistic studies on the ruthenium WOCs have clarified several issues important for WOC optimization.[39,55−58]

Our aim is to design WOCs that have the stability advantages of heterogeneous metal oxides with all the other advantages of the soluble WOCs (readily studied, optimized, and formulated). To this end we recently reported the Rb_8K_2 salt of a new polyanion, $[\{Ru_4O_4(OH)_2(H_2O)_4\}(\gamma\text{-}SiW_{10}O_{36})_2]^{10-}$, free of organic structure, that exhibits several reversible one-electron redox couples by cyclic voltammetry and catalyzes both the electrooxidation and chemical oxidation of water in aqueous solution at low overpotentials.[59] Henceforth the polyanion is "**1(0)**" and the full complex is "**Rb_8K_2-1(0)**" for simplicity. The polytungstate ligands, $\gamma\text{-}SiW_{10}O_{36}^{8-}$, of **1(0)** stabilize the Ru_4O_6 core over several oxidation states needed for catalytic water oxidation and are themselves oxidatively, hydrolytically, and thermally stable.[60−62] At the same time, the salts of **1(0)** are molecular and soluble and thus amenable to detailed and insightful structural, mechanistic, and computational investigations. Simultaneously and completely independently, Sartorel et al. (Bonchio and co-workers) prepared a different salt of the same polyanion catalyst via another synthetic route.[63] These two reports are distinguished by the oxidant, pH of catalysis, and the salt used to obtain the X-ray structure: our study used $[Ru(bpy)_3]^{3+}$ as the oxidant buffered at pH 7[59] and Sartorel et al.[63] used Ce^{4+} as the oxidant at pH ∼1.8.[63] A similar Ru_4O_6 polytungstate structure was reported by Mizuno and co-workers,

(13) Kanan, M. W.; Surendranath, Y.; Nocera, D. G. *Chem. Soc. Rev.* **2009**, *38*, 109–114.
(14) Lutterman, D. A.; Surendranath, Y.; Nocera, D. G. *J. Am. Chem. Soc.* **2009**, *131*, 3838–3839.
(15) Youngblood, W. J.; Lee, S.-H. A.; Kobayashi, Y.; Hernandez-Pagan, E. A.; Hoertz, P. G.; Moore, T. A.; Moore, A. L.; Gust, D.; Mallouk, T. E. *J. Am. Chem. Soc.* **2009**, *131*, 926–927.
(16) Lehn, J. M.; Sauvage, J. P.; Ziesel, R. *Nouv. J. Chim.* **1979**, *3*, 423–427.
(17) Gersten, S. W.; Samuels, G. J.; Meyer, T. J. *J. Am. Chem. Soc.* **1982**, *104*, 4029–4030.
(18) Gilbert, J. A.; Eggleston, D. S.; Wyatt, R. M., Jr.; Geselowitz, D. A.; Gersten, S. W.; Hodgson, D. J.; Meyer, T. J. *J. Am. Chem. Soc.* **1985**, *107*, 3855–3864.
(19) Comte, P.; Nazeeruddin, M. K.; Rotzinger, F. P.; Frank, A. J.; Grätzel, M. *J. Mol. Catal.* **1989**, *52*, 63–84.
(20) Schoonover, J. R.; Ni, J.; Roecker, L.; White, P. S.; Meyer, T. J. *Inorg. Chem.* **1996**, *35*, 5885–5892.
(21) Rüttinger, W.; Dismukes, G. C. *Chem. Rev.* **1996**, *97*, 1–24.
(22) Limburg, J.; Vrettos, J. S.; Liable-Sands, L. M.; Rheingold, A. L.; Crabtree, R. H.; Brudvig, G. W. *Science* **1999**, *283*, 1524–1527.
(23) Wada, T.; Tsuge, K.; Tanaka, K. *Angew. Chem., Int. Ed.* **2000**, *39*, 1479–1482.
(24) Sens, C.; Romero, I.; Rodríguez, M.; Llobet, A.; Parella, T.; Benet-Buchholz, J. *J. Am. Chem. Soc.* **2004**, *126*, 7798–7799.
(25) Chen, H.; Faller, J. W.; Crabtree, R. H.; Brudvig, G. W. *J. Am. Chem. Soc.* **2004**, *126*, 7345–7349.
(26) Hurst, J. K. *Coord. Chem. Rev.* **2005**, *249*, 313–328.
(27) Zong, R.; Thummel, R. *J. Am. Chem. Soc.* **2005**, *127*, 12802–12803.
(28) Yang, X.; Baik, M.-H. *J. Am. Chem. Soc.* **2006**, *128*, 7476–7485.
(29) Tagore, R.; Chen, H.; Zhang, H.; Crabtree, R. H.; Brudvig, G. W. *Inorg. Chim. Acta* **2007**, *360*, 2983–2989.
(30) Tagore, R.; Crabtree, R. H.; Brudvig, G. W. *Inorg. Chem.* **2007**, *46*, 2193–2203.
(31) McDaniel, N. D.; Coughlin, F. J.; Tinker, L. L.; Bernhard, S. *J. Am. Chem. Soc.* **2008**, *130*, 210–217.
(32) Tagore, R.; Crabtree, R. H.; Brudvig, G. W. *Inorg. Chem.* **2008**, *47*, 1815–1823.
(33) Brimblecombe, R.; Swiegers, G. F.; Dismukes, G. C.; Spiccia, L. *Angew. Chem., Int. Ed.* **2008**, *47*, 7335–7338.
(34) Siegbahn, P. E. M. *Inorg. Chem.* **2008**, *47*, 1779–1786.
(35) Liu, F.; Concepcion, J. J.; Jurss, J. W.; Cardolaccia, T.; Templeton, J. L.; Meyer, T. J. *Inorg. Chem.* **2008**, *47*, 1727–1752.
(36) Hurst, J. K.; Cape, J. L.; Clark, A. E.; Das, S.; Qin, C. *Inorg. Chem.* **2008**, *47*, 1753–1764.
(37) Deng, Z.; Tseng, H.-W.; Zong, R.; Wang, D.; Thummel, R. *Inorg. Chem.* **2008**, *47*, 1835–1848.
(38) Romero, I.; Rodríguez, M.; Sens, C.; Mola, J.; Kollipara, M. R.; Francàs, L.; Mas-Marza, E.; Escriche, L.; Llobet, A. *Inorg. Chem.* **2008**, *47*, 1824–1834.
(39) Concepcion, J. J.; Jurss, J. W.; Templeton, J. L.; Meyer, T. J. *Proc. Nat. Acad. Sci. U.S.A.* **2008**, *105*, 17632–17635.
(40) Concepcion, J. J.; Jurss, J. W.; Templeton, J. L.; Meyer, T. J. *J. Am. Chem. Soc.* **2008**, *130*, 16462–16463.
(41) Sala, X.; Romero, I.; Rodriguez, M.; Escriche, L.; Llobet, A. *Angew. Chem., Int. Ed.* **2009**, *48*, 2842–2852.
(42) Romain, S.; Bozoglian, F.; Sala, X.; Llobet, A. *J. Am. Chem. Soc.* **2009**, *131*, 2768–2769.
(43) Hull, J. F.; Balcells, D.; Blakemore, J. D.; Incarvito, C. D.; Eisenstein, O.; Brudvig, G. W.; Crabtree, R. H. *J. Am. Chem. Soc.* **2009**, *131*, 8730–8731.
(44) Kunkely, H.; Vogler, A. *Angew. Chem., Int. Ed.* **2009**, *48*, 1685–1687.
(45) Xu, Y.; Åkermark, T.; Gyollai, V.; Zou, D.; Eriksson, L.; Duan, L.; Zhang, R.; Åkermark, B.; Sun, L. *Inorg. Chem.* **2009**, *48*, 2717–2719.
(46) Development of the Mn-based WOCs was aided by considerable work establishing the geometrical and electronic structures of other synthetic multi-manganase complexes.[53,100−105]
(47) Ferreira, K. N.; Iverson, T. M.; Maghlaoui, K.; Barber, J.; Iwata, S. *Science* **2004**, *303*, 1831–1838.
(48) Barber, J. *Inorg. Chem.* **2008**, *47*, 1700–1710.
(49) Yano, J.; Kern, J.; Sauer, K.; Latimer, M. J.; Pushkar, Y.; Biesiadka, J.; Loll, B.; Saenger, W.; Messinger, J.; Zouni, A.; Yachandra, V. K. *Science* **2006**, *314*, 821–825.
(50) Yano, J.; Yachandra, V. K. *Inorg. Chem.* **2008**, *47*, 1711–1726.
(51) Yeagle, G. J.; Gilchrist, M. L.; McCarrick, R. M.; Britt, R. *Inorg. Chem.* **2008**, *47*, 1803–1814.
(52) Rotzinger, F. P.; Munavalli, S.; Comte, P.; Hurst, J. K.; Gratzel, M.; Pern, F.-J.; Frank, A. J. *J. Am. Chem. Soc.* **1987**, *109*, 6619–6626.
(53) Yagi, M.; Kaneko, M. *Chem. Rev.* **2001**, *101*, 21–35.
(54) Muckerman, J. T.; Polyansky, D. E.; Wada, T.; Tanaka, K.; Fujita, E. *Inorg. Chem.* **2008**, *47*, 1787–1802.
(55) Chronister, C. W.; Binstead, R. A.; Ni, J.; Meyer, T. J. *Inorg. Chem.* **1997**, *36*, 3814–3815.
(56) Binstead, R. A.; Chronister, C. W.; Ni, J.; Hartshorn, C. M.; Meyer, T. J. *J. Am. Chem. Soc.* **2000**, *122*, 8464–8473.
(57) Yamada, H.; Koike, T.; Hurst, J. K. *J. Am. Chem. Soc.* **2001**, *123*, 12775–12780.
(58) Yamada, H.; Siems, W. F.; Koike, T.; Hurst, J. K. *J. Am. Chem. Soc.* **2004**, *126*, 9786–9795.
(59) Geletii, Y. V.; Botar, B.; Kögerler, P.; Hillesheim, D. A.; Musaev, D. G.; Hill, C. L. *Angew. Chem., Int. Ed.* **2008**, *47*, 3896–3899.
(60) *Polyoxometalates: From Platonic Solids to Anti-retroviral Activity*; Pope, M. T., Müller, A., Eds.; Kluwer Academic Publishers: Dordrecht, Netherlands, 1993.
(61) Hill, C. L.; Prosser-McCartha, C. M. *Coord. Chem. Rev.* **1995**, *143*, 407–455.
(62) Neumann, R. *Prog. Inorg. Chem.* **1998**, *47*, 317–370.
(63) Sartorel, A.; Carraro, M.; Scorrano, G.; Zorzi, R. De; Geremia, S.; McDaniel, N. D.; Bernhard, S.; Bonchio, M. *J. Am. Chem. Soc.* **2008**, *130*, 5006–5007.

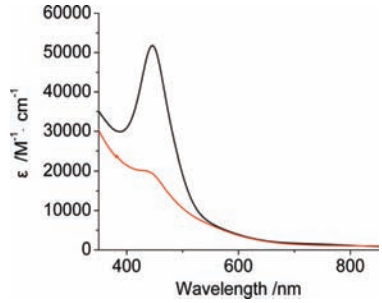

Figure 1. UV−vis spectra of **Rb_8K_2-1(0)** (black) and **$H_2Ce_{2.5}K(NH_4)_{0.5}$-1(+1)** (red) in 0.1 M HCl.

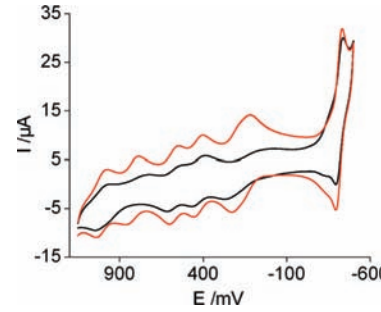

Figure 2. Cyclic voltammograms of 0.7 mM **Rb_8K_2-1(0)** (black curve) and 0.7 mM **$H_2Ce_{2.5}K(NH_4)_{0.5}$-1(+1)** (red curve) in 0.1 M HCl. Scan rate 25 mV/s. The differences in the peak positions are due to differences in ion-pairing and the effect of electrolyte on interfacial electron transfer.

but no catalytic or other properties were reported.[64] Recently we communicated visible light-driven water oxidation catalyzed by **1(0)** in the presence of a sacrificial electron acceptor (persulfate)[65] and a second polyoxometalate (POM)-based WOC, $K_{14}[(IrCl_4)KP_2W_{20}O_{72}]$, which unlike **1(0)** is hydrolytically unstable.[66]

We report here the extensive characterization of **1(0)** and related ruthenium-substituted polytungstates to help one understand water oxidation catalyzed by the different salts of polyanion **1(0)**. The geometric and electronic structures, redox and spectroscopic features, and water oxidation mechanism are addressed.

Results and Discussion

One-Electron Oxidized Form of Water Oxidation Catalyst $Rb_8K_2[\{Ru_4O_4(OH)_2(H_2O)_4\}(\gamma\text{-}SiW_{10}O_{36})_2]$ (or Rb_8K_2-1(0)) and Related Compounds. We have prepared and thoroughly characterized this one-electron oxidized complex and two other multiruthenium polytungstates related to polyanion **1(0)** that were reported earlier.[59] For simplicity and discussion purposes, we have used the following notation throughout the paper: the multiruthenium polytungstates are identified by a number followed by their charge/oxidation state relative to the parent polyanion, $[\{Ru_4O_4(OH)_2(H_2O)_4\}(\gamma\text{-}SiW_{10}O_{36})_2]^{10-}$, or **1(0)**, in parentheses. Thus, this parent polyanion, with four Ru(IV) centers, is **1(0)**, and its analogous one-electron-reduced and four-electron-oxidized polyanions, for example, are **1(−1)** and **1(+4)**, respectively. The cations (counterions) that define the full complex precede the number separated by a hyphen; thus, the original Rb_8K_2 salt of **1(0)** is **Rb_8K_2-1(0)**. These letter-number identifiers refer to both protonated and deprotonated forms of the complexes.

$[\{Ru^{V}Ru^{IV}_3O_6(OH_2)_4\}(\gamma\text{-}SiW_{10}O_{36})_2]^{11-}$, (1(+1)). When a 2.2-fold molar excess of Ce(IV) is present over the $RuCl_3$ reactant in the synthesis of **1(0)**, the one-electron-oxidized $Ru(IV)_3Ru(V)$ form of **1(0)**, or **1(+1)**, and specifically **$H_2Ce_{2.5}K(NH_4)_{0.5}$-1(+1)**, can be isolated. The UV−vis spectra and cyclic voltammograms of **Rb_8K_2-1(0)** are compared with those for **$H_2Ce_{2.5}K(NH_4)_{0.5}$-1(+1)** in Figures 1 and 2.

We have also prepared and characterized the water-soluble Cs salt of the diruthenium complex, $Cs_6[\{Ru_2O_2(OH_2)_2\}(\gamma\text{-}SiW_{10}O_{36})]\cdot 25H_2O$ (or **Cs_6-2**), whose organic-solvent-soluble tetrabutylammonium (TBA) salt we reported earlier,[67] and another polymorph of the tetrachloro derivative of polyanion **1(0)** that was reported last year by Mizuno and co-workers.[64] The latter complex is the $[H_2N(CH_3)_2]_8K_2H_2$ salt of the polyanion isostructural to **1(0)** but with the terminal ruthenium aqua ligands replaced by chloride ligands. We have determined that polyanion **2** is oxidized by air (O_2) in water to **1(0)** via eq 1. All of the chemistry of these two complexes is given in Supporting Information.

$$2[\{Ru^{III}_2O_2(OH_2)_2\}(\gamma\text{-}SiW_{10}O_{36})]^{6-} + O_2 + 2H^+ \rightarrow [\{Ru^{IV}_4O_4(OH)_2(H_2O)_4\}(\gamma\text{-}SiW_{10}O_{36})_2]^{10-} \quad (1)$$

X-ray Crystal Structures of the Tetraruthenium Polytungstates. The X-ray structures of **Rb_8K_2-1(0)**[59] and **$H_2Ce_{2.5}K(NH_4)_{0.5}$-1(+1)** show that both polyanions, **1(0)** and **1(+1)**, are very similar: D_{2d} polyanions with $[Ru_4O_6]$ cores of approximately T_d local symmetry sandwiched between two symmetry-equivalent tetradentate $[\gamma\text{-}SiW_{10}O_{36}]^{8-}$ ligands. All the Ru centers in the three structures are out of pocket, i.e., the rutheniums are not bonded to the central heteroatom oxygens. The same is true of the tetrachloro derivative (polyanion is **Cl_4-1(0)** and the full complex is **$[H_2N(CH_3)_2]_8K_2H_2$-Cl_4-1(0)**). The crystal data and refinement parameters for **$H_2Ce_{2.5}K(NH_4)_{0.5}$-1(+1)** and **$[H_2N(CH_3)_2]_8K_2H_2$-Cl_4-1(0)** are summarized in Table 3 (Experimental Section), and the structure of polyanion **1(+1)** is given in Figure 3. Despite the near structural congruity of polyanions **1(0)** and **1(+1)**, there are noteworthy differences in bond lengths and angles that reflect differing protonation of the $[Ru_4O_6]$ oxygens and different oxidation states of the Ru centers. The protonation state of the six bridging oxygens in the $[Ru_4O_6]$ core can be distinguished by bond valence sum (BVS) calculations. Both **Rb_8K_2-1(0)**[59] and the related complex, **Cs_{10}-1(0)**, of Sartorel et al.[63] were reported to have two of these Ru-O-Ru oxygens protonated. In polyanion **1(+1)**, none of these $[Ru_4O_6]$ core oxygens are protonated, which is understandable given the lower negative electron density on this $[Ru_4O_6]$ core compared with that in **1(0)**. All four ruthenium terminal ligands in **1(+1)** remain aqua as in **1(0)** and not hydroxo. Protonation of Ru−O−Ru oxygens is consistent with simple charge arguments along with considerable X-ray structural and reactivity work on other POMs[68−71] indicating these oxygen sites would be more basic than the W^{VI}-O-Ru^{IV} and W^{VI}-O-W^{VI} oxygen sites.

(64) Yamaguchi, S.; Uehara, K.; Kamata, K.; Yamaguchi, K.; Mizuno, N. *Chem. Lett.* **2008**, *37*, 328–329.
(65) Geletii, Y. V.; Huang, Z.; Hou, Y.; Musaev, D. G.; Lian, T.; Hill, C. L. *J. Am. Chem. Soc.* **2009**, *131*, 7522–7523.
(66) Cao, R.; Ma, H.; Geletii, Y. V.; Hardcastle, K. I.; Hill, C. L. *Inorg. Chem.* **2009**, *48*, 5596–5598.
(67) Quiñonero, D.; Wang, Y.; Morokuma, K.; Khavrutskii, L. A.; Botar, B.; Geletii, Y. V.; Hill, C. L.; Musaev, D. G. *J. Phys. Chem.* **2006**, *110*, 170–173.
(68) Day, V. W.; Klemperer, W. G.; Schwartz, C. *J. Am. Chem. Soc.* **1987**, *109*, 6030–6044.

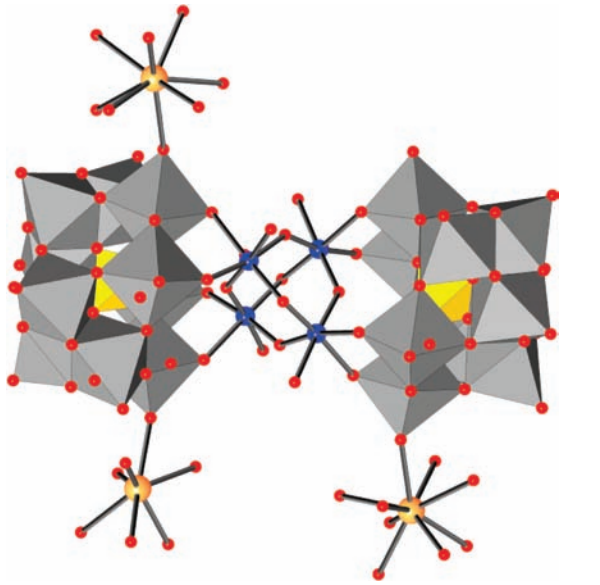

Figure 3. X-ray structure of $\mathbf{H_2Ce_{2.5}K(NH_4)_{0.5}\text{-}1(+1)}$ in combined polyhedral (polytungstate ligands) and ball-and-stick notation (the Ce atoms and the central Ru_4O_6 core). Ru: blue; O: red; Ce: orange; WO_6 octahedra: gray; SiO_4 tetrahedra: yellow. Hydrogen atoms, water molecules, and the potassium cations (not coordinated to the POM) are omitted for clarity.

Ruthenium Oxidation State Assignments in 1(0), Cl_4-1(0), and 1(+1). There are six arguments that the four ruthenium centers in polyanions **1(0)** and **Cl_4-1(0)** are d^4 Ru(IV): (1) the voltammetric rest potentials (additional studies are addressed below), (2) calculated BVS values for these atoms, (3) full elemental analysis indicating the counterions in the unit cell (charge balancing the polyanion), (4) the diamagnetism of the complex, (5) lack of EPR signal, and (6) formation of both **1(0)** and **Cl_4-1(0)** requires oxidation of the $RuCl_3$ reactant (no product is formed when either reaction is run under an argon atmosphere). Similarly, there are multiple arguments that the tetraruthenium core in **1(+1)** is one electron more oxidized than that in **1(0)** or **Cl_4-1(0)**, namely, $[Ru^{IV}{}_3Ru^{V}]$. First, production of **1(+1)** from **1(0)** requires an excess of Ce(IV) (Ce(IV) oxidizes some chloride present, a quite favorable process thermodynamically). Second, BVS calculations on all four Ru centers yield oxidation states of 4.21, 4,24, 4.26, and 4.38 (average 4.27; the sum is 17.09) consistent with one-electron oxidation of the $[Ru(IV)_4]$ core in **1(0)**. This charge is delocalized over all four Ru centers on the X-ray data collection time scale. (Note there are four symmetry-distinct Ru centers because $\mathbf{H_2Ce_{2.5}K(NH_4)_{0.5}\text{-}1(+1)}$ crystallizes in the triclinic *P*-1 space group in contrast to $\mathbf{Rb_8K_2\text{-}1(0)}$, which has two distinct Ru centers in the unit cell.) Third (related to point 2), the Ru···Ru separations in $\mathbf{H_2Ce_{2.5}K(NH_4)_{0.5}\text{-}1(+1)}$ (3.42−3.44 Å) are significantly smaller than those in $\mathbf{Rb_8K_2\text{-}1(0)}$ (3.47−3.66 Å). Fourth, the oxidation state assignment of a $[Ru^{IV}{}_3Ru^{V}]$ core was confirmed by back-titration of $\mathbf{H_2Ce_{2.5}K(NH_4)_{0.5}\text{-}1(+1)}$ with the reductant Sn(II) to polyanion **1(0)**. Fifth, Figure 1 clearly shows that the UV−vis spectra of the two complexes are distinct from one another.

(69) Pope, M. T. *Heteropoly and Isopoly Oxometalates*; Springer-Verlag: Berlin, 1983.
(70) Hill, C. L. In *Comprehensive Coordination Chemistry-II: From Biology to Nanotechnology*; Wedd, A. G., Ed.; Elsevier Ltd.: Oxford, UK, 2004; Vol. 4, pp 679−759.
(71) Villa, E. M.; André, O. C.; Balogh, E.; Anderson, T. M.; Nyman, M. D.; Casey, W. H. *Angew. Chem., Int. Ed.* **2008**, *47*, 4844–4846.

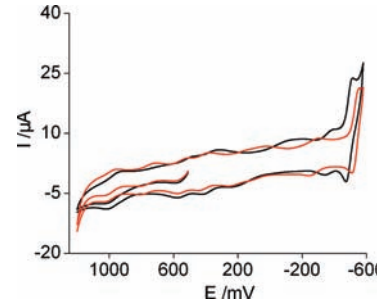

Figure 4. Cyclic voltammograms of 0.7 mM $\mathbf{Rb_8K_2\text{-}1(0)}$ in 0.2 M lithium sulfate buffer at pH 2.0 (black curve) and in the presence of 0.58 M KCl (red curve). Scan rate 25 mV/s.

Table 1. Potentials of Anodic (E_a) and Cathodic (E_c) Peaks in Cyclic Voltammograms of 0.7 mM $\mathbf{Rb_8K_2\text{-}1(0)}$[a]

pH = 2 (0.2 M lithium sulfate buffer)			0.1 M HCl		
$E_{1/2}$	E_a	E_c	$E_{1/2}$	E_a	E_c
973	1010	935	1012	1045	980
∼749	∼830	667	809	856	762
529	580	479	581	615	547
370	428	312	424	458	390
30	235	−175	154	272	35
−365	−335	−395	−310	−255	−365
−499	−458	−540	−415	−382	−447

[a] Values versus Ag/AgCl (3 M NaCl) reference electrode.

Electrochemistry of Polyanions 1(n) and the Effect of Alkali Metal Cations. Cyclic voltammograms of aqueous solutions of **1(0)** are pH and ionic strength dependent (Figures 4 and S4, Table 1). At pH 2.0 in 0.2 M lithium sulfate buffer, four cathodic peaks are well separated in the positive domain, a broad peak is also seen at ca. −175 mV, while the peak at ca. −395 mV overlaps with an intense peak of W(VI/V) reduction at ca. −540 mV. At a lower pH in 0.1 M HCl, peaks in the positive domain are shifted to more positive values, and the difference between cathodic and anodic potentials moves closer to 60 mV. The replacement of 0.2 M lithium sulfate buffer with 0.1 M HCl results in a very large shift of the broad cathodic wave from ca. −175 to ca. 35 mV. Thus, at low alkali metal cation concentration at acidic pH, seven quasi-reversible waves are observed in the range from 1.05 to −0.55 V. These waves are assigned to the following couples: **1(+2)/1(+1)**, **1(+1)/1(+0)**, **1(+0)/1(−1)**, **1(−1)/1(−2)**, **1(−2)/1(−4)**, (two broad converged 1-electron peaks) **1(−4)/1(−5)**, **1(−5)/1(−6)**. Reduction of W(VI) to W(V) takes place in the last couple. The data are summarized in Table 1.

Addition of alkali metal cations (as chloride or other salts) also changes the shape and position of reduction and oxidation peaks. The weakest effect is seen with LiCl and the strongest with KCl. In general, the peaks become better separated and shift to more positive potentials. The shifts are more pronounced for the peaks at lower potentials. The broad cathodic and anodic peaks (−175 and 235 mV, respectively) split into two separate peaks and shift to higher potentials. Two adjoining anodic peaks at the highest potential (ca. 830 and 1010 mV) become well separated. The peak at ca. −395 mV (overlapping with an intense peak for W(VI/V) reduction at ca. −540 mV) also shifts to more positive values, while the last peak (corresponding to the tungsten reduction) shifts slightly to a more negative value.

The voltammetric peaks depend on the nature and concentration of cations present, and this effect is more pronounced for the more reduced POMs (more negative **n**, in polyanion, **1(n)**).

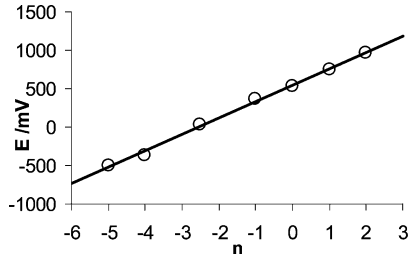

Figure 5. Reduction potentials of **1(n)/1(n − 1)** couples, $E_{1/2} = (E_a + E_c)/2$, as a function of **n** determined from cyclic voltammograms of 0.7 mM **Rb_8K_2-1(0)** in 0.2 M lithium sulfate buffer (pH 2.0). $E_{1/2}$ (mV) = $214n + 546$, $R^2 = 0.997$.

While these findings are consistent with ion pairing at more negative potentials (more reduced polyanions),[72−77] the voltammetric behavior at more positive potentials cannot be explained exclusively by ion pairing.

When the experimentally determined reduction potentials of the **1(n)/1(n − 1)** couples, $E_{1/2} = (E_a + E_c)/2$, are plotted as a function of **n**, the number electrons added or removed from the polyanion, a very good linear dependence is observed (Figure 5).[78] The slopes of $E_{1/2}$ as a function of **n** are 214 and 210 mV per one unit change of **n** in 0.2 M lithium sulfate buffer (pH 2.0) and in 0.1 M HCl, respectively. Interestingly for **n** in the range from +2 to −4, the redox processes are associated with changes in oxidation states of ruthenium, but the most negative value, **n** = −5, which is assigned to the W(VI)/(V) reduction, also lies on the same line.

The linear dependence of the several successive oxidation and reduction potentials, as in the case of **1(0)**, is referred to as a Coulomb staircase, which is a classical feature of a charging capacitor (e.g., an electrode surface). While seen in large molecules including C_{60} and platinum carbonyl clusters (26−38 atoms)[79,80] as well as some gold nanoclusters around 1 nm in diameter,[81−83] a Coulomb staircase is only rarely observed for molecular systems where electronic coupling usually dictates unevenly spaced potentials. Interestingly, Au nanoparticles revert to molecule-like behavior for clusters under 20 kDa (around 100 gold atoms), and these systems can be modeled as an ensemble of electrode/electrolyte solution/molecule capacitors.[79−84]

The "bulk material-like" behavior of **1(0)** can be linked to its unusual electronic structure. Frontier orbital analysis (performed at the RI-DFT level of theory) indicates that its HOMO orbitals are very closely spaced in energy and largely involve the $[Ru_4O_6]$ core (see Figure S11 in Supporting Information). An analogous situation is operable for the LUMO orbitals. The HOMO−LUMO energy gap is calculated to be only 0.316 eV. Thus, the $[Ru_4O_6]$ core and WO bonding and antibonding orbitals provide a quasi-continuum of frontier orbitals similar to that observed around the Fermi level of a conducting solid. The observed "quasi-continuum" nature of the **1(0)** frontier orbitals correlates with the reported oxidation and reduction features and explains the unusual Coulomb staircase of redox processes in the cyclic voltammetry of **1(0)**. These closely spaced potentials are one key to a WOC with redox leveling, i.e. the ability to undergo at least four one-electron oxidation state changes over a narrow range under turnover conditions.

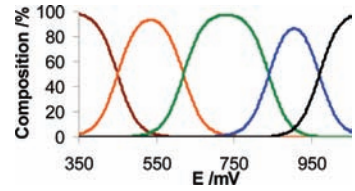

Figure 6. Speciation of **1(n)** as a function of the electrochemical potential of the solution in 0.1 M H_2SO_4. Black: **1(+2)**, blue: **1(+1)**, green: **1(0)**, orange: **1(−1)**, brown: **1(−2)**.

Potentiometric titration of **1(−2)** by Ce(IV) also shows four successive one-electron oxidation steps with reduction potentials of 0.47, 0.62, 0.85, and 0.97 V (in 0.1 M H_2SO_4) for the **1(+2)/1(+1)**, **1(+1)/1(0)**, **1(0)/1(−1)**, **1(−1)/1(−2)** couples, respectively. The backward titration by Sn(II) to reduce **1(+2)** to **1(−2)** confirms the perfect chemical reversibility of these redox processes. Details of titration data acquisition are given in the Experimental Section and Supporting Information. On the basis of the reduction potentials (from both cyclic voltammetry and potentiometric titration), we generated a speciation diagram, plotting the percentage of **1(n)** present in solution as a function of the electrochemical potential of the solution (Figure 6). As a consequence, a simple measurement of the solution potential identifies which **1(n)** is present in a given solution. However, this technique does not produce reliable results at low concentrations relevant to catalytic water oxidation conditions, where UV−vis spectroscopy can be more useful. The UV−vis spectra of **1(n)**, with **n** in the range from −2 to +2, were obtained from potentiometric titrations in 0.1 M H_2SO_4 and are shown in Figure 7. The same titration spectra in 0.1 M HCl are given in Figure S8 in Supporting Information.

Catalytic Water Oxidation. In the initial communication[59] we reported that micromolar concentrations of **Rb_8K_2-1(0)** catalyze eq 2, O_2 is produced in yields of up to ∼66% based on $[Ru(bpy)_3]^{3+}$, and H_2O is the source of oxygen atoms in O_2 (using ^{18}O-labeled water). Equation 2 is thermodynamically favorable over a wide pH range: E^o for $[Ru(bpy)_3]^{3+}/[Ru(bpy)_3]^{2+}$ is 1.24 V vs NHE and E^o for water oxidation to O_2 is 0.82 V vs NHE at pH 7. Here we thoroughly examine eq 2 catalyzed by **1(0)**.

(72) Grigoriev, V. A.; Hill, C. L.; Weinstock, I. A. *J. Am. Chem. Soc.* **2000**, *122*, 3544–3545.
(73) Grigoriev, V. A.; Cheng, D.; Hill, C. L.; Weinstock, I. A. *J. Am. Chem. Soc.* **2001**, *123*, 5292–5307.
(74) Keita, B.; Mbomekalle, I. M.; Lu, Y. W.; Nadjo, L.; Berthet, P.; Anderson, T. M.; Hill, C. L. *Eur. J. Inorg. Chem.* **2004**, 3462–3475.
(75) Casey, W. H. *Chem. Rev.* **2006**, *106*, 1–16.
(76) Anderson, T. M.; Thoma, S. G.; Bonhomme, F.; Rodriguez, M. A.; Park, H.; Parise, J. B.; Alam, T. M.; Larentzos, J. P.; Nyman, M. *Cryst. Growth Des.* **2007**, *7*, 719–723.
(77) Antonio, M. R.; Nyman, M.; Anderson, T. M. *Angew. Chem., Int. Ed.* **2009**, *48*, 6136–6140.
(78) The broad peak with $E_a = 235$ mV and $E_c = -175$ mV is assigned to the couple **1(2)/1(−4)**; **n** is given an average value−2.5.
(79) Roth, J. D.; Lewis, G. J.; Safford, L. K.; Jiang, X.; Dahl, L. F.; Weaver, M. J. *J. Am. Chem. Soc.* **1992**, *114*, 6159–6169.
(80) Weaver, M. J.; Gao, X. *J. Phys. Chem.* **1993**, *97*, 332–338.
(81) Ingram, R. S.; Hostetler, M. J.; Murray, R. W.; Schaaff, T. G.; Khoury, T.; Whetten, R. L.; Bigioni, T. P.; Guthrie, D. K.; First, P. N. *J. Am. Chem. Soc.* **1997**, *119*, 9279–9280.
(82) Chen, S.; Murray, R. W.; Feldberg, S. W. *J. Phys. Chem. B* **1998**, *102*, 9898–9907.
(83) Chen, S.; Ingram, R. S. H.; Hostetler, M. J.; Pietron, J. J.; Murray, R. W.; Schaaff, T. G.; Khoury, J. T.; Alvarez, M. M.; Whetten, R. L. *Science* **1998**, *120*, 2098–2101.
(84) The spacing between the potentials (ΔV) gives access to the equivalent capacity of the system ($C = e/\Delta V$ where e is the charge of the electron). For **1(0)**, $C = 0.75$ aF. This value is somewhat higher than systems noted in the text (0.3 aF for C_{60}, 0.45 aF for the platinum clusters, and 0.5−0.6 aF for the gold nanoclusters) likely because of the higher dielectric constant of our aqueous solution compared to the organic solvents used in the other cases.

$$4[Ru(bpy)_3]^{3+} + 2H_2O \rightarrow 4[Ru(bpy)_3]^{2+} + O_2 + 4H^+ \quad (2)$$

1. O_2 Yields and Turnover Number (TON). Table 2 summarizes the effect of catalyst and oxidant concentration on O_2 yields and TON. The dependence of O_2 yield on catalyst concentration (Table 2, runs 1−5) obeys a hyperbolic function: $Y(\%) = [\mathbf{1(0)}]/([\mathbf{1(0)}] + 0.021\ \mu M)$, where $Y = (100\%) \times 4O_2/[Ru(bpy)_3]^{3+}$ and $[\mathbf{1(0)}]$ is the catalyst concentration expressed in μM. The turnover number (TON) $= [O_2]/[\mathbf{1(0)}]$ decreases with increasing $[\mathbf{1(0)}]$. Such dependences suggest that $[Ru(bpy)_3]^{3+}$ is consumed in two parallel pathways: (a) catalytic water oxidation in eq 2 and (b) self-decomposition, very likely via bpy ligand oxidation (eq 3, where (bpy)′ is an oxidatively modified bpy).[85]

$$2[Ru(bpy)_3]^{3+} \rightarrow Ru(bpy)_3]^{2+} + [Ru(bpy)_2(bpy)']^{2+} \quad (3)$$

An increase of initial $[Ru(bpy)_3]^{3+}$ concentration from 0.6 to 2.3 mM results in a significant and almost linear decrease in O_2 yield, from 65% to 18% (Table 2, runs 3, 6, and 7). The $[Ru(bpy)_3]^{3+}$ decomposition side reaction is very complex, and its rate quickly increases with $[Ru(bpy)_3]^{3+}$ concentration.[4] Therefore, at constant catalyst concentration, this side reaction prevails over the catalytic water oxidation pathway. The addition of $[Ru(bpy)_3]^{2+}$ to the catalytic system slightly decreases the O_2 yield (Table 2, runs 4, 9, and 10). Addition of 0.06 mM free bpy ligand increases the O_2 yield from 50% to 54% (Table 2, runs 3 and 12), but this effect is within experimental error.

As noted above, the addition of LiCl, NaCl, and KCl to **Rb_8K_2-1(0)** solutions significantly changes the voltammograms at both acidic and neutral pH values, with the strongest effect observed for K^+. A similar alkali metal cation concentration effect is seen on catalytic O_2 evolution (eq 2). Addition of 100 mM NaCl or KCl results in a modest drop or a major (50%) drop in O_2 yield, respectively (Table 2, runs 3, 13, and 14). Replacing sodium cations with lithium cations in the phosphate buffer only slightly increases the yield from 50% to 54%, but this effect is within experimental error. A minimal effect would be expected given the documented relative ion pairing association constants for these alkali metal cations and POMs (K^+, strongest pairing > Na^+ > Li^+).[70,72−74,76,77] In unbuffered solutions of polyanion **1(0)** and $[Ru(bpy)_3]^{3+}$ (initial pH ∼3.5), the O_2 yield increases slightly from 50% to 65%, but the overall reaction time increases by 1 order of magnitude (runs 3 and 8). On the basis of the data in Table 2 we attempted to maximize TON, i.e., $[O_2]/[\mathbf{1(0)}]$, and achieved a value of ca. 10^2 (run 15). We compared the activities of **Rb_8K_2-1(0)** and an equimolar quantity of $RuCl_3$ (a plausible precursor of RuO_2). The O_2 yield using the latter was with experimental error the same as the O_2 detection level.

2. Kinetics of $[Ru(bpy)_3]^{3+}$ Reduction. Figure 8 shows that addition of catalyst, **Rb_8K_2-1(0)**, significantly increases the reduction rate of $[Ru(bpy)_3]^{3+}$,which is consistent with the hyperbolic dependence of O_2 yield on catalyst concentration stated above. The reaction kinetics are very complex. The reaction starts very quickly but then noticeably slows down (Figure 9). The kinetic curves do not obey any simple rate law, e.g., mono- or biexponential. Addition of $[Ru(bpy)_3]^{2+}$ to the catalytic system has a complex effect: it inhibits the fast initial step (Figure S10 in Supporting Information), but the overall reaction is completed in a shorter time. The addition of small amounts of free bpy has a negligible effect on reaction kinetics.

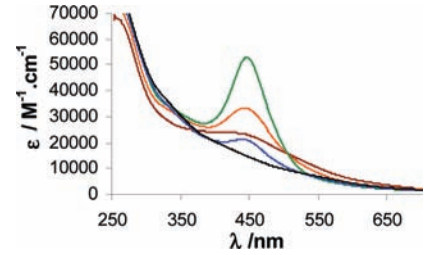

Figure 7. UV−vis spectra of **1(n)** complexes in 0.1 M H_2SO_4. Black: **1(+2)**, blue: **1(+1)**, green: **1(0)**, orange: **1(−1)**, brown: **1(−2)**.

Figure 10 shows the effect of alkali metal cation (as Li, Na, or K phosphate buffers) on the kinetics of catalytic $Ru(bpy)_3^{3+}$ reduction (Li^+ fastest < Na^+ < K^+ slowest). This effect parallels the alkali metal cation dependence of the voltammetric behavior of **Rb_8K_2-1(0)** and the O_2 yields in catalytic water oxidation. Thus, the data on reaction kinetics are consistent with the data on catalytic O_2 yields.

Energetics and Intermediates in the Water Oxidation Process. Initially[59] we believed that polyanion **1(+2)** could be reduced by water to **1(−2)** in a concerted 4-electron process thus releasing O_2. At low pH using Ce(IV) (CAN) as an oxidant, Sartorel et al.[63] reported a catalyst turnover frequency (TOF) for their **Cs_{10}-1(0)** of 0.01−0.1 s^{-1}, implying that a reactive intermediate is long-lived (10−100 s). The **1(+2)/1(+1)** couple in the voltammogram of **Rb_8K_2-1(0)** at pH 1−2 is reversible with a very well-defined cathodic feature at scan rate 25 mV/s, indicating that the lifetime of polyanion **1(+2)** is >10 s, which is consistent with the experimentally observed TOF. However, the potential for the overall 4-electron reduction of **1(+2)** to **1(−2)** is ∼0.7 V (0.95 V versus NHE), Table 1, and thus considerably lower than that required for the 4-electron oxidation of H_2O to O_2 (∼1.17 V versus NHE at pH 1.0, the approximate pH of a separate study[63]). Assuming that the linear correlation of reduction potentials of **1(n)/1(n − 1)** couples we documented (Figure 5) is valid for **n** > 2 with a slope of ∼0.21 V per one unit of **n**, the potential for overall 4-electron reduction of **1(+3)** to **1(−1)** would be ∼1.17 V (NHE), which is thermodynamically neutral for water oxidation. However, the estimated potential for **1(+4)** to **1(0)** couple is 1.38 V (NHE), making water oxidation more favorable thermodynamically. From the same linear dependence the estimated reduction potential of the **1(+4)/1(+3)** couple is ∼1.45 V (versus NHE), which is accessible if Ce(IV) is used as an oxidant (E^o for $Ce(OH)^{3+}/Ce_{aq}^{3+}$ is 1.72 V NHE[86]). Thus, under very acidic conditions the water oxidizing polyanion is likely to be **1(+4)** formed in four successive one-electron oxidations of **1(0)** by Ce^{4+}.

At neutral pH, that used in our catalytic water oxidation studies,[59,65,66] the voltammetric data are not informative. However, the potentials of the **1(n)/1(n − 1)** couples can be estimated assuming a linear dependence of these potentials versus **n** is also applicable and that **n** is directly related to the charge of **1(n)** polyanions. With these assumptions, this linear dependence on **n** can be simply interpreted as a dependence on

(85) The reaction rate in eq 3 is pH-dependent; the reaction mechanism is very complex and not fully understood. Ligand oxidation probably starts as an intramolecular process and converts bpy to a radical that is further oxidized by a second $[Ru(bpy)_3]^{3+}$. Thus, two $[Ru(bpy)_3]^{3+}$ are involved in eq 3.

(86) Pourbaix, M. *Atlas d'équilibres électrochimiques*; Gauthier-Villars: Paris, 1963.

Table 2. Effect of Catalyst, Oxidant Concentration, and Ionic Interactions on O_2 Yield and Turnover Number (TON) in the Oxidation of Water by $[Ru(bpy)_3]^{3+}$ Catalyzed with $\mathbf{Rb_8K_2}$**-1(0)**[a]

run	[**1(0)**], μM	$[Ru(bpy)_3]^{3+}$, mM (μmol)	buffer[b], mM	others, mM	O_2, μmol[c]	Y[d], %	TON[e]
1	0[f]	1.15 (9.1)	20		<0.15	<7	
2	1	1.15 (9.1)	20		0.73	32	91
3	2	1.15 (9.1)	20		1.14	50	73
4	5	1.15 (9.1)	20		1.57	69	39
5	8	1.15 (9.1)	20		1.7	75	30
6	2	0.6 (4.8)	20		0.78	65	49
7	2	2.3 (18.4)	20		0.82	18	51
8	2[g]	1.15 (9.1)	0		1.48	65	92
9	5	1.15 (9.1)	20	0.4, $[Ru(bpy)_3]^{2+}$	1.39	61	35
10	5	1.15 (9.1)	20	0.8, $[Ru(bpy)_3]^{2+}$	1.28	56	32
11	2	1.15 (9.1)	20 (Li)		1.23	54	76
12	2	1.15 (9.1)	20	0.06, bpy	1.23	54	76
13	2	1.15 (9.1)	20	100, NaCl	0.96	42	60
14	2	1.15 (9.1)	20 (K)	100, KCl	0.59	26	37.5
15	1	1.15 (9.1)	10 (Li)	0.06, bpy	0.75	33	92
16	0	1.15 (9.1)	20	0.008, $RuCl_3$	<0.25	<11	

[a] Conditions: total reaction volume 8 mL, initial pH 7.2, (final pH 6.2−6.6), 24 ± 2 °C. [b] Sodium phosphate unless otherwise indicated. [c] Typical experimental error ca. ±0.2 μmol O_2. [d] $Y = 4[O_2]/[[Ru(bpy)_3]^{3+}]$. [e] TON = $n_{O2}/n_{\mathbf{1(0)}}$. [f] Reaction is complete in ∼15 min. [g] Reaction is complete in ∼75 min, final pH ∼3.5.

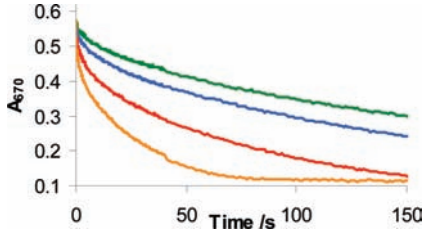

Figure 8. Effect of catalyst concentration on kinetics of $[Ru(bpy)_3]^{3+}$ reduction measured as a decrease in absorbance at 670 nm. [$\mathbf{Rb_8K_2}$**-1(0)**] = 0 (green curve), 3 (blue curve), 5 (red curve), and 8 μM (orange curve). Conditions: 1.2 mM $[Ru(bpy)_3]^{3+}$ in 25 mM potassium phosphate buffer, pH 7.2, 25 °C.

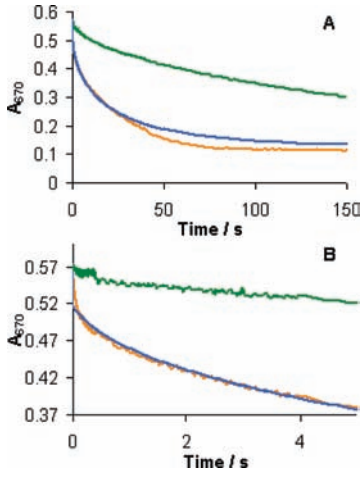

Figure 9. Kinetics of $[Ru(bpy)_3]^{3+}$ reduction to $[Ru(bpy)_3]^{2+}$ measured as a decrease in absorbance at 670 nm at two different time-scales. Green = noncatalyzed, orange = experimental data, and blue = fit. Conditions: 1.2 mM $[Ru(bpy)_3]^{3+}$, 8 μM $\mathbf{Rb_8K_2}$**-1(0)**, 20 mM sodium phosphate buffer, pH 7.2, 25 °C.

the charge of **1(n)** complexes. Charge is one of five factors that dictate POMs potentials in solution.[70] At pH < 2, the charge of polyanion **1(n)** is 10^-. At pH > 5, **1(0)** releases two protons[59] and its charge decreases by two units to become 12^-. If the linear correlation of the reduction potentials versus the polyanion charge remains applicable, then the reduction potentials for **1(n)**/**1(n − 1)** couples should be 2 × 0.21 = 0.42 V lower at neutral pH than in acidic media. Hence, the estimated overall 4-electron

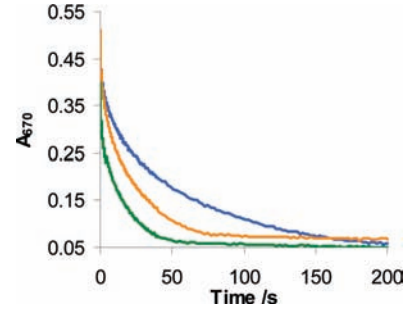

Figure 10. Effect of alkaline cations in phosphate buffer on kinetics of $[Ru(bpy)_3]^{3+}$ reduction measured as a decrease in absorbance at 670 nm. Conditions: 1.2 mM $[Ru(bpy)_3]^{3+}$, 5 μM $\mathbf{Rb_8K_2}$**-1(0)**, 25 mM potassium (blue curve), sodium (orange curve), or lithium (green curve) phosphate buffer, pH 7.2, 25 °C.

reduction potential of the **1(+4)/1(0)** couple becomes ∼0.95 V at neutral pH (versus NHE), which is higher than the potential required for the 4-electron water oxidation to O_2 (∼0.82 V at pH 7.0). From the same linear dependence the estimated reduction potential of the **1(+4)/1(+3)** couple is ∼1.25 V (versus NHE), which is equal to E^o for the $[Ru(bpy)_3]^{3+}/[Ru(bpy)_3]^{2+}$ couple, 1.24 V vs NHE.[87] Consequently, it is reasonable to assume that, at neutral pH, the water oxidizing reactive intermediate is also the **1(+4)** polyanion but in the deprotonated form. The last step, oxidation of polyanion **1(+3)** to **1(+4)** by $[Ru(bpy)_3]^{3+}$, is a thermodynamically neutral reaction and therefore should be a reversible step. The irreversible oxidation of water by the **1(+4)** is the driving force for the overall reaction in eq 2 and makes this process thermodynamically favorable.

Kinetic Model of Water Oxidation. On the basis of the reaction thermodynamic and kinetic information in the previous sections and mechanistic studies by Meyer[35,55,56] and Hurst[26,36,58] on water oxidation by the blue dimer, we suggest eqs 4−8 as the likely mechanism for water oxidation by $[Ru(bpy)_3]^{3+}$ catalyzed by **1(0)**:

(87) *CRC Handbook of Chemistry and Physics*, 81st ed.; Lide, D. R., Ed.; CRC Press: Boca Raton, FL, 2000.

$$\mathbf{1(0)} + [Ru(bpy)_3]^{3+} \rightarrow \mathbf{1(+1)} + [Ru(bpy)_3]^{2+} \quad \text{fast} \qquad (4)$$

$$\mathbf{1(+1)} + [Ru(bpy)_3]^{3+} \rightarrow \mathbf{1(+2)} + [Ru(bpy)_3]^{2+} \quad \text{fast} \qquad (5)$$

$$\mathbf{1(+2)} + [Ru(bpy)_3]^{3+} \rightarrow \mathbf{1(+3)} + [Ru(bpy)_3]^{2+} \quad \text{fast} \qquad (6)$$

$$\mathbf{1(+3)} + [Ru(bpy)_3]^{3+} = \mathbf{1(+4)} + [Ru(bpy)_3]^{2+} \quad K \qquad (7)$$

$$\mathbf{1(+4)} \rightarrow \mathbf{1(0)} + O_2 \quad k_{cat} \qquad (8)$$

Equations 4−6 are thermodynamically very favorable and therefore are assumed to proceed rapidly. Equilibrium 7 is a reversible electron transfer between oppositely charged species with an equilibrium constant K and is assumed to be established quickly (steady-state assumption). Consequently, the steady state concentrations of polyanions **1(0)**, **1(+1)**, and **1(+2)** are negligible compared to those of **1(+3)** and **1(+4)**. The latter two complexes are in equilibrium because the electron transfer reaction in eq 7 is estimated to be thermoneutral (see above). The rate-limiting step is assumed to be eq 8, which is presented in a very simplified manner. Equation 8 may have a complex mechanism involving the catalyst and solvent water molecules; its apparent rate constant for purposes of kinetic analysis is simply given as k_{cat}. If an oxygen atom(s) from **1(+4)** is used to form O_2, then **1(+4)** is not reduced directly to **1(0)** but to some intermediate, which in turn reacts with water to regenerate **1(0)**. Assuming steady state conditions for **1(+3)** and **1(+4)** and accounting for mass balance with respect to all **1(n)** polyanions, we derive the reaction rate law shown in eq 9, where [**1**] is the total analytical concentration of the catalyst and [Ru^{2+}] and [Ru^{3+}] are the concentrations of $[Ru(bpy)_3]^{2+}$ and $[Ru(bpy)_3]^{3+}$, respectively:

$$\text{rate} = -\frac{d[Ru^{3+}]}{dt} = 4k_{cat}[\mathbf{1}]\frac{1}{1 + \frac{1}{K}\frac{[Ru^{2+}]}{[Ru^{3+}]}} \qquad (9)$$

$$\left(1 - \frac{1}{K}\right)([Ru^{3+}] - [Ru^{3+}]_0) + \frac{[Ru^{3+}]_0}{K}\ln\frac{[Ru^{3+}]}{[Ru^{3+}]_0} = -4k_{cat}[\mathbf{1}]t \qquad (10)$$

$$(1 - K)\frac{A_0 - A}{A_0 - A_\infty} + \ln\frac{A - A_\infty}{A_0 - A_\infty} = -4k_{cat}[\mathbf{1}]\frac{K}{[Ru^{3+}]_0}t \qquad (11)$$

The integration of eq 9 results in eq 10, which links the $[Ru(bpy)_3]^{3+}$ concentration with the reaction time. Since the reaction product, $[Ru(bpy)_3]^{2+}$, as well as the catalyst absorb light at 670 nm ($\varepsilon = 5\ M^{-1}\ cm^{-1}$ for $[Ru(bpy)_3]^{2+}$, $\varepsilon = 2.0 \times 10^3\ M^{-1}\ cm^{-1}$ for **1(0)**), $[Ru(bpy)_3]^{3+}$ concentration is not linearly proportional to absorbance at 670 nm (A_{670}). Consequently, eq 10 was converted to eq 11 to describe the dependence of A_{670} on reaction time. The rate law in eq 9 (and hence eqs 10 and 11) was obtained by ignoring the self-decomposition of $[Ru(bpy)_3]^{3+}$ (eq 3). Thus, the fitting of experimental kinetic data, A_{670} versus time, to eq 11 with K and k_{cat} as variable parameters was performed at high catalyst concentrations. Details are described in Supporting Information. An example is given in Figure 9: the best fit is obtained using $K = 2$ and $k_{cat} = 0.25\ s^{-1}$. Deviations from the experimental curve at the very beginning of the reactions are due to the assumption that eqs 4−7 are very fast. The noncatalytic self-decomposition of $[Ru(bpy)_3]^{3+}$ results in deviations at high reaction conversions. Therefore, these deviations are considered to be acceptable.

The proposed mechanism is in good agreement with most experimental observations. For example, the value $K = 2$ is consistent with the expected thermodynamics of the reaction in eq 7 (approximately thermoneutral). Varying the initial $[Ru(bpy)_3]^{3+}$ concentration has no effect on the reaction rate vs conversion (Figure S9 in Supporting Information) in accordance with eq 9. Indeed, the reaction rate depends on the ratio of the concentration of $[Ru(bpy)_3]^{2+}$ to $[Ru(bpy)_3]^{3+}$ but not on the initial concentration of $[Ru(bpy)_3]^{3+}$ (if the initial concentration of $[Ru(bpy)_3]^{2+}$ is equal to zero). At the same time, addition of $[Ru(bpy)_3]^{2+}$ to the catalytic mixture at the beginning of the reaction decreases the initial reaction rate, Figure S10 in Supporting Information. However, at higher conversions the reaction rate increases with an increase of total $[Ru(bpy)_3]^{2+}$ concentration, probably due to the well-known acceleration by $[Ru(bpy)_3]^{2+}$ of $[Ru(bpy)_3]^{3+}$ self-decomposition.[4]

Several alternative reaction mechanisms have also been analyzed and subsequently ruled out (see Supporting Information). For example, making one of the one-electron oxidation steps rate-determining would require a simple exponential decay of the $[Ru(bpy)_3]^{3+}$ concentration. Alternatively, one could propose H_2O oxidation to O_2 by **1(+3)**. However this process is thermodynamically unfavorable (vide supra). In addition, a rate-limiting **1(+3)** + 2 $H_2O \rightarrow O_2 + 4H^+ +$ **1(−1)** requires the kinetics of $[Ru(bpy)_3]^{3+}$ consumption to be zero order and that is not what is observed.

Stability of 1(n) in Solutions and under Catalytic Turnover Conditions. Six complementary experiments or observations confirm that **1(0)** is stable in solution at natural pH (3−4 depending on concentration) and under catalytic turnover conditions. Details of these experiments are given in Supporting Information. First and second, **1(0)** is shown to be hydrolytically stable. Both UV−vis spectra and cyclic voltammograms show no change in solutions of **Rb_8K_2-1(0)** after several months of storage at ambient temperature and room illumination (**Rb_8K_2-1(0)** decomposes very slowly in 0.1 M HCl solution at ambient temperature). Third, the equivalent molar quantity of $RuCl_3$, a precursor of known water oxidation catalyst RuO_2 was far less catalytically active than **Rb_8K_2-1(0)** (Table 2, run 16). Fourth, no particles indicative of RuO_2 or other possible decomposition products were observed in postcatalysis solutions by small-angle X-ray scattering (SAXS; Cu Kα radiation). Fifth, no particles <500 nm were observed in these solutions by dynamic light scattering (293 K, 100 s, ALV correlator with HeNe laser; $\lambda =$ 632.8 nm). Sixth, voltammetric monitoring of the catalyst in solution after catalysis showed the same enhancement of the catalytic current for oxidation of $[Ru(bpy)_3]^{2+}$ to $[Ru(bpy)_3]^{3+}$ (Figure S6 in Supporting Information).

The 1- and 2-electron reduced polyanions, **1(−1)** and **1(−2)**, are slowly oxidized by O_2 (in 0.1 M HCl, 0.1 M HNO_3, or in sulfate buffer at pH 2), but the reaction does not proceed completely to **1(0).** The first step, the oxidation of **1(−2)** to **1(−1)**, while slow ($t_{1/2} \sim 10$ h), is almost an order of magnitude faster than the following step, oxidation **1(−1)** to **1(0)**. Detailed kinetic studies of these processes are in progress. The two-electron oxidized specie, **1(+2)**, is spontaneously reduced by water to **1(+1)** in 0.1 M aqueous HNO_3 at an elevated temperature (45 °C) in ∼10−15 h, but the reaction does not proceed completely to **1(0)**. Spontaneous reduction of **1(+1)** to **1(0)** by water is significantly slower. The time-dependent

UV−vis spectroscopic data are shown in Figure S7 in Supporting Information. Interestingly, if 0.1 M HNO_3 is replaced with 0.1 M HCl, the reaction becomes several times faster, probably due to Cl^- oxidation to Cl_2 (identified by its characteristic sharp smell).

Experimental Section

Materials and Methods. Potassium γ-decatungstosilicate, $K_8[\gamma\text{-}SiW_{10}O_{36}]\cdot 12H_2O$[88] and $Rb_8K_2[\{Ru^{IV}_4O_4(OH)_2(H_2O)_4\}(\gamma\text{-}SiW_{10}O_{36})_2]\cdot 25H_2O$ (**Rb_8K_2-1(0)**)[59] were prepared by the literature methods. Synthesis and characterization of the new polymorph of $[H_2N(CH_3)_2]_8K_2H_2[\{Ru_4O_2(OH)_4Cl_4\}(\gamma\text{-}SiW_{10}O_{36})_2]$ (**$[H_2N(CH_3)_2]_8K_2H_2Cl_4$-1(0)**) are given in Supporting Information. Elemental analyses were performed by Columbia Analytical Services (Tucson, AZ) and Atlantic Microlab Inc. (Norcross, GA). Water for the preparation of solutions was obtained from a Barnstead Nanopure water-purification system, and all other chemicals and salts were from commercial sources. $[Ru(bpy)_3]^{3+}$ was obtained by oxidation of $[Ru(bpy)_3]Cl_2$ with PbO_2 in 0.5 M H_2SO_4 and precipitated from a solution by adding concentrated $HClO_4$.[3,89] The product was dried under vacuum and stored in a freezer (~4 °C) in a sealed vial. Aqueous stock solutions of $[Ru(bpy)_3]^{3+}$, 0.5−2.5 mM, at natural pH (~3) were used immediately after preparation. The concentrations of $[Ru(bpy)_3]^{3+}$ and $[Ru(bpy)_3]^{2+}$ in solution were determined by UV−vis from the absorbance at 670 nm ($\varepsilon = 4.2 \times 10^2$ M^{-1} cm^{-1}) and at 454 nm ($\varepsilon = 1.45 \times 10^4$ M^{-1} cm^{-1}), respectively. Contamination of $[Ru(bpy)_3]^{3+}$ with $[Ru(bpy)_3]^{2+}$ never exceeded 3−5%.[59] Infrared spectra (2% sample in KBr) were recorded on a Nicolet 510 FTIR spectrometer. UV−vis spectra were acquired using an Agilent 8453 spectrophotomer equipped with a diode-array detector and with a magnetic stirrer and temperature controller (Agilent 89090A). The spectra were recorded in a 10 mm two-neck quartz cell with a stopper and a stopcock under Ar, air, or O_2. ^{183}W (20.8 MHz) and ^{29}Si (75.6 MHz) NMR spectra were obtained at 300 K in 10 mm o.d. tubes on a Bruker DRX500 spectrometer equipped with a BBO probehead. The chemical shifts are given with respect to a 2 M aqueous solution of sodium tungstate and tetramethylsilane, respectively, and are measured by the substitution method. For ^{183}W NMR, a saturated aqueous solution of the dodecatungstosilicic acid, $\alpha\text{-}H_4SiW_{12}O_{40}$ ($\delta = -103.8$ ppm) was used as secondary standard. The sample was prepared by dissolving ca. 1.2 g of **Rb_8K_2-1(0)** in 2 mL of saturated lithium perchlorate solution and 0.5 mL of D_2O. The resulting insoluble $KClO_4$ and $RbClO_4$ were removed by filtration. Electrochemical data were obtained at room temperature using a BAS CV-50W electrochemical analyzer equipped with a glassy-carbon working electrode, a Pt-wire auxiliary electrode, and a Ag/AgCl (3 M NaCl) BAS reference electrode. All reduction potentials are measured relative to this reference electrode (~250 mV difference between the NHE and BAS electrodes; this value may vary slightly depending on solution acidity and ionic strength). Cyclic voltammograms (CVs) were obtained under Ar using 0.5−2 mM POM concentrations in 0.1 M HCl, 0.1 M H_2SO_4, 10−200 mM sulfate buffer (pH 2.0), or 10−200 mM phosphate buffer (pH 7.2) with scan rates of 25 and 100 mV s^{-1}. Sulfate buffers were prepared from H_2SO_4 and LiOH, NaOH, or KOH. Phosphate buffers were prepared from H_3PO_4 and NaOH or KOH. The appropriate amounts of LiCl, NaCl, or KCl were added to buffer solutions to examine the effect of differing cations.

CV was also used to evaluate catalyst stability. In this series of experiments, the voltammograms of 1.15 mM $[Ru(bpy)_3]Cl_2$ were recorded in 20 mM sodium phosphate buffer containing 0.2 M NaCl (total volume 8 mL), then 0.08 mL of 0.5 mM **Rb_8K_2-1(0)** was added, giving a 5 μM solution of polyanion **1(0)**. The CV of this solution was recorded again, and these voltammograms were compared with those of a "post-reaction solution." The catalytic water oxidation reaction was carried out as described below with $[Ru(bpy)_3](ClO_4)_3$ as an oxidant under the same concentration conditions, but NaCl was not present. When the reaction was completed (the solution color changed from green to orange), NaCl was added and CV was recorded. The data are presented in Figure S6 in Supporting Information.

Aqueous solutions of reduced/oxidized **1** were prepared by bulk electrolysis under Ar using a reticulated vitreous-carbon working electrode. The auxiliary electrode, a coiled Pt-wire, was located in a separate compartment connected by fritted glass. The reactions were carried out in 0.1 M HCl or 0.1 M H_2SO_4 solutions. During electrolysis, vigorous mixing was provided by a magnetic stirrer and by agitation caused from the bubbling of Ar gas through the solution (air was rigorously excluded). The working electrode was typically set at a potential ~170 mV more negative/positive than that of the redox couple (measured by CV in the same solution) of the desired reduction/oxidation process. The reaction progress was monitored continuously by the number of coulombs of charge passed through the solution. In most cases, with POM concentrations of ca. 0.7−1.6 mM, the total charge transferred, Q, was 30−60% higher than theoretical ($Q = nFN$, where $n = 1$ or 2, F is the Faraday constant and N is [POM] × V, where V is the total solution volume)[90]

Synthesis of Oxidized Complex, $H_2Ce_{2.5}K(NH_4)_{0.5}[\{Ru^VRu^{IV}_3O_6(OH_2)_4\}(\gamma\text{-}SiW_{10}O_{36})_2]\cdot 33H_2O$ ($H_2Ce_{2.5}K(NH_4)_{0.5}$-1(+1)). To a vigorously stirred solution of 2.0 g (0.67 mmol) of $K_8[\gamma\text{-}SiW_{10}O_{36}]\cdot 12H_2O$ in 32.5 mL of water was added 0.3 g (1.33 mmol) of solid $RuCl_3\cdot H_2O$. The pH of the dark brown solution was lowered from 3 to 1.65 by adding several drops of 4 M HCl. After 5 min of stirring, a solution of 1.6 g (2.9 mmol) of $Ce(NH_4)_2(NO_3)_6$ (CAN) dissolved in 10 mL of 0.1 M HCl was added dropwise. The solution was then filtered and allowed to stand in a 50 mL beaker open to air. The first crystals formed within a few hours. Dark crystalline **$H_2Ce_{2.5}K(NH_4)_{0.5}$-1(+1)** (350 mg; 0.054 mmol, 8% based on W) was collected after 4 days. IR (KBr) ν_{max} (cm^{-1}): 483 (w), 539 (m), 573 (m), 688 (m), 780 (s), 804 (s), 864 (s), 912 (m), 945 (m), 999 (w), 1025 (w), 1411 (w), 3200 (br sh). UV−vis spectrum in 0.1 M HNO_3 had the same characteristic peak at 445 nm but with $\varepsilon_{445} = 2 \times 10^4$ M^{-1} cm^{-1}, which is ~2.3 times lower than for **Rb_8K_2-1(0)** (Figure 1). Cyclic voltammograms of **$H_2Ce_{2.5}K(NH_4)_{0.5}$-1(+1)** in 0.1 M HCl were similar to that of **Rb_8K_2-1(0)** showing six reversible peaks but at slightly more positive potentials (Figure 2). Anal Calcd. for **$H_2Ce_{2.5}K(NH_4)_{0.5}[\{Ru^VRu^{IV}_3O_6(OH_2)_4\}(\gamma\text{-}SiW_{10}O_{36})_2]\cdot 33\,H_2O$**: Si, 0.9; Ru, 6.3; W, 56.9; K, 0.6; Ce, 5.4; N, 0.1. Found: Si, 1.0; Ru, 6.2; W, 54.1; K, 0.7; Ce, 5.2; N, 0.16.

Preparation of Polyanions 1(−1) and 1(−2). The reduced POMs are obtained in solution by adding 0.5 or 1 equiv of $SnSO_4$ (0.05−0.1 M aqueous solutions in 0.1 M HNO_3 or 0.1 M H_2SO_4). Solutions of Sn(II) are unstable under air, and therefore all manipulations were performed under Ar. Alternatively, bulk electrolysis of **Rb_8K_2-1(0)** in solutions at low pH (0.1 M HCl or H_2SO_4) under constant reduction potential was also used to prepare the 1- and 2-electron-reduced forms of **1(0)**.

Spontaneous Reduction of 1(+1) and 1(+2) in Acidic Aqueous Solutions. Solutions of **1(+2)**, 20 and 40 μM, were made using crystalline samples of **Rb_8K_2-1(0)** dissolved in 0.1 M H_2SO_4 or in 0.1 M HNO_3. Two equivalents of CAN were then added to the above solution to quickly oxidize **1(0)** to **1(+2)**. This was observed as a decrease in absorbance at 445 nm. Time-elapsed UV−vis spectroscopy was consequently performed at 45 °C using these oxidized species. The representative data are shown in Figure S7 in Supporting Information. A similar experiment was done using

(88) Tézé, A.; Hervé, G. In *Inorganic Syntheses*; Ginsberg, A. P., Ed.; John Wiley and Sons: New York, 1990; Vol. 27, pp 85−96.

(89) Shafirovich, V. Ya.; Strelets, V. V. *Bull. Acad. Sci. USSR, Div. Chem. Sci. (Engl. Transl.)* **1980**, 7–12.

(90) At low POM concentrations (ca. 1 mM), background currents (reduction of H^+ at low pHs) might significantly contribute to the total current transferred during electrolysis.

Table 3. Crystal Data and Refinement Parameters for the X-ray Structures of $H_2Ce_{2.5}K(NH_4)_{0.5}$-**1(+1)** and $[H_2N(CH_3)_2]_8K_2H_2Cl_4$-**1(0)**

complex	$H_2Ce_{2.5}K(NH_4)_{0.5}$-1(+1)	$[H_2N(CH_3)_2]_8K_2H_2Cl_4$-1(0)
molecular formula	$Ce_{2.5}H_{78}N_{0.5}KO_{115}Ru_4Si_2W_{20}$	$C_{16}H_{78}Cl_4N_8K_2O_{82}Ru_4Si_2W_{20}$
formula wt (g mol^{-1})	6504.33	6052.32
temperature (K)	173(2)	173(2)
radiation (λ, Å)	0.71073	0.71073
crystal system	triclinic	triclinic
space group	*P*-1 (No. 2)	*P*-1 (No. 2)
a (Å)	16.083(3)	14.7305(8)
b (Å)	18.405(4)	19.6144(9)
c (Å)	20.111(4)	20.8418(10)
α (deg)	102.564(10)	100.745(3)
β (deg)	99.400(10)	99.569(3)
γ (deg)	91.116(11)	94.958(3)
volume (Å^3)	5723.2(19)	5790.9(5)
Z	2	2
μ (mm^{-1})	21.662	20.551
F(000)	5747	5352
crystal size (mm^3)	0.18 × 0.11 × 0.08	0.22 × 0.06 × 0.03
reflections collected	90897	81223
independent reflections	23311 [*R*(int) = 0.0734]	22562 [*R*(int) = 0.1329]
absorption correction	semiempirical from equivalents	semiempirical from equivalents
refinement method	full-matrix least-squares on F^2	full-matrix least-squares on F^2
goodness-of-fit on F^2	1.008	1.015
final *R* indices	$R_1{}^a$ = 0.0541	$R_1{}^a$ = 0.0897
[$R > 2\sigma(I)$]	$wR_2{}^b$ = 0.1867	$wR_2{}^b$ = 0.2436
R indices (all data)	$R_1{}^a$ = 0.0634	$R_1{}^a$ = 0.1799
	$wR_2{}^b$ = 0.1961	$wR_2{}^b$ = 0.3063

^{a} $R_1 = \Sigma||F_o| - |F_c||/|F_o|$. ^{b} $wR_2 = \{\Sigma[w(F_o^2 - F_c^2)^2]/\Sigma[w(F_o^2)^2]\}^{0.5}$.

crystalline $H_2Ce_{2.5}K(NH_4)_{0.5}$-**1(+1)** (no CAN was added in this case). The appearance of the characteristic peak at 445 nm with time indicates spontaneous reduction of polyanions **1(+1)** and **1(+2)**.

X-ray Crystallography. Complete data sets for $H_2Ce_{2.5}K(NH_4)_{0.5}$-**1(+1)** ($Ce_{2.5}H_{78}N_{0.5}KO_{115}Ru_4Si_2W_{20}$) and $[H_2N(CH_3)_2]_8K_2H_2$-Cl_4-**1(0)** ($C_{16}H_{78}Cl_4N_8K_2O_{82}Ru_4Si_2W_{20}$) were collected at Emory University. Single crystals of each of these compounds suitable for X-ray analysis were coated with Paratone-N oil, suspended in a small fiber loop, and placed in a cooled gas stream on a Brüker D8 SMART APEX2 CCD sealed tube diffractometer. Diffraction intensities were measured using graphite monochromated Mo Kα radiation (λ = 0.71073 Å) at 173(2) K and a combination of ϕ and ω scans with 10 s frames at 0.5° increments were taken. Data collection, indexing, and initial cell refinements were carried out using APEX2;[91] frame integration and final cell refinements were done using SAINT.[92] The molecular structure of each complex was determined using direct methods and Fourier techniques and refined by full-matrix least-squares. A multiple absorption correction, including face indexed absorption correction, was applied using the program SADABS.[93] The largest residual electron density for each structure was located close to (less than 1.0 Å from) the countercation or tungsten atoms and was most likely due to imperfect absorption corrections frequently encountered in heavy-metal atom structures. All heavy atoms, including Ce, K, Si, Cl, Ru, and W, were refined anisotropically. Scattering factors and anomalous dispersion corrections are taken from the *International Tables for X-ray Crystallography*. Structure solution, refinement, graphic and generation of publication materials were performed by using SHELXTL, V6.14 software.[94] Refinement details and structural parameters are summarized in Table 3.

Potentiometric and UV−vis Titrations. Stock solutions of polyanion **1(−2)** were prepared by bulk electrolysis of 1.6 mM Rb_8K_2-**1(0)** (160 mg, 2.4 mmol, in 15 mL of either 0.1 M HCl or 0.1 M H_2SO_4) at a potential of 200 mV (see above). Alternatively, a solution of **1(−2)** can be prepared by the two-electron reduction of **1(0)** using $SnSO_4$. The UV−vis spectra and oxidation potentials of resulting stock solutions of **1(−2)** under Ar do not change on the time scale of the titration experiment. Typically, 10 mL of the solution was then titrated by adding 70 μL increments of a 24 mM CAN solution prepared in 0.1 M HCl or 0.1 M H_2SO_4. After each addition, the solution potential was measured using a Pt-redox electrode (SympHony epoxy combination redox electrode with the internal Ag/AgCl reference electrode, VWR Scientific Products). At the same time, 40 μL aliquots were withdrawn and diluted by addition of 3 mL of 0.1 M acid (HCl, H_2SO_4 or HNO_3) to record the UV−vis spectra. The measured values of solution potentials were then plotted versus the number of Ce(IV) equivalents added per mole or initial polyanion **1(−2)**. In several experiments after adding 5−6 equiv of CAN, the solution was gradually titrated back to **1(−2)** by Sn(II). All procedures were performed under Ar. Simulation of the potentiometric curves was achieved using the standard Nernst equation, eq 12.

$$E_{n,n-1} = E^{app}_{n,n-1} + \frac{RT}{F}\ln\left(\frac{[\mathbf{1(n)}]}{[\mathbf{1(n-1)}]}\right) \quad \mathbf{n} = -1, 0, 1, 2 \tag{12}$$

The $E^{app}_{n,n-1}$ potentials were determined by a manual adjustment of the $E^{app}_{n,n-1}$ values to obtain the best visually satisfying fit between simulated and experimental data. All data were corrected for a dilution factor. The $E^{app}_{n,n-1}$ values are the apparent potentials at constant ionic strength and pH.

Effect of Li^+, Na^+, and K^+ Cations on Reduction Potentials of 1(0). The effect of different cations (LiCl, NaCl, and KCl were used) on the CV reduction/oxidation peaks was studied in 0.1 M HCl, as well as at pH 2.0 (0.2 M lithium, sodium or potassium sulfate buffer) and at pH 7.2 (0.1 M sodium or potassium phosphate buffers). In a typical experiment, 1.9 mg (2.8 μmol, 0.7 mM) of Rb_8K_2-**1(0)** was dissolved in 4 mL of 0.2 M lithium sulfate buffer, and its CV was recorded between 1.2 and (−0.58) V (vs Ag/AgCl) at scan rate 25 mV s^{-1}. Then, 0.1 mL of a 2.9 M solution of LiCl or solid LiCl was added. The CVs were recorded after each addition. The same procedure was used to determine the effect of sodium or potassium cations (Figure 5) by adding NaCl or KCl to the solution of Rb_8K_2-**1(0)** in 0.2 M sodium or potassium sulfate

(91) *Bruker APEX2*; Bruker AXS Inc.: Madison, WI, 2007.
(92) *Bruker SAINT*; Bruker AXS Inc.: Madison, WI, 2007.
(93) *Bruker SADABS*; Bruker AXS Inc.: Madison, WI, 2007.
(94) Sheldrick, G. M. *Acta Crystallogr.* **2008**, *A64*, 112–122.

buffer (pH 2.0), 0.1 M HCl, or 0.1 M sodium or potassium phosphate buffers (pH 7.2).

Catalytic Water Oxidation, O_2 Measurements. The same protocols were used as in previous reports.[59,65,66] O_2 was quantified by gas chromatography using a HP5890A gas chromatograph equipped with a 5 Å molecular sieve column and thermal conductivity detector with Ar as the carrier gas. Vessels and syringes were airtight. All details, including sources of error, are given in Supporting Information.

Kinetics of $[Ru(bpy)_3]^{3+}$ Reduction. The reactions were studied using a Hi-Tech KinetAsyst Stopped Flow SF-61SX2 instrument equipped with a diode array detector operating in wavelength range 400−700 nm. One of the feeding syringes was filled with $[Ru(bpy)_3]^{3+}$ solutions, and the other with a catalytic solution. Each data set included 200 spectra collected with different time scales: from 0−0.4 s up to 0−400 s. Typically, the consumption of $[Ru(bpy)_3]^{3+}$ was followed by a decrease in absorbance at 670 nm ($\varepsilon_{670} = 4.2 \times 10^2$ M^{-1} cm^{-1}) with optical path length $l = 10$ mm. Alternatively, the reaction was followed by formation of $[Ru(bpy)_3]^{2+}$ (increase in absorbance in the range 440−500 nm) with optical path length $l = 1$ mm. The data were acquired and treated using KinetAsyst 3.0. Detailed analysis of kinetic data was performed using both Gepasi v 3.30 software[95] and Solver subprogram in Microsoft Excel. Details are given in Supporting Information.

Computational Procedures. All calculations were performed using the Turbomole program.[96] The geometries of these species were optimized without any symmetry constraints at the RI-PBE level. In these calculations we used the triple-ζ plus polarization (TZVP) basis sets[97] for all atoms together with 28-electron relativistic effective core potentials (28e-RECP) for Ru and W from the Stuttgart group.[98] Solvent effects were taken into account using the Conductor-like Screening Model (COSMO)[99] with water as a solvent ($R_{solvent} = 1.30$ Å) and the following atomic radii in Å: O, 1.720; H, 1.300; Si, 2.458; Ru, W, 2.2225.

Conclusions

1. The compound **$H_2Ce_{2.5}K(NH_4)_{0.5}[\{Ru^{V}Ru^{IV}_3O_6(OH_2)_4\}(\gamma\text{-}SiW_{10}O_{36})_2]$** (or **$H_2Ce_{2.5}K(NH_4)_{0.5}$-1(+1)**) has been prepared and characterized by X-ray crystallography and several other techniques. It contains a polyanion, **1(+1)**, that is one-electron more oxidized than the polyanion, **1(0)**, in the parent water oxidation catalyst.

2. The rest potentials, X-ray structure/BVS calculations, full elemental analysis, magnetism (diamagnetic), EPR, and requirement of an oxidant (O_2) are all consistent with $[Ru^{IV}_4O_6]$ and $[Ru^{V}Ru^{IV}_3O_6]$ cores in polyanions **1(0)** and **1(+1)**, respectively.

3. Cyclic voltammetric and potentiometric titrations establish the potentials of the **1(+2)/1(+1)**, **1(+1)/1(0)**, **1(0)/1(−1)**, **1(−1)/1(−2)** couples of **1(0)**, and a speciation diagram, plotting the percentage of **1(n)** present in solution as a function of the electrochemical potential of the solution, is calculated (Figure 6). The potentials depend on the nature and concentration of counterions, primarily because of ion pairing.

4. DFT calculations show very small energy differences between the low-lying frontier orbitals of **1(0)**, results that parallel the experimental finding of seven reversible couples by cyclic voltammetry with four of them occurring over range of ca. 0.5 V in the H_2O/O_2 potential region. The potentials are evenly spaced (a Coulomb staircase), more consistent with bulk-like properties.

5. Water oxidation by $[Ru(bpy)_3]^{3+}$ catalyzed by **1(0)** shows a hyperbolic dependence of O_2 yield on catalyst concentration consistent with competing water and ligand (bpy) oxidations. Addition of $[Ru(bpy)_3]^{2+}$, or separately, the more strongly ion pairing cations, decreases the O_2 yield. The kinetics of water oxidation assessed by reduction of the $[Ru(bpy)_3]^{3+}$ chromophore are very complex, but the O_2 yields and rate law data are consistent.

6. An analysis of energetics of water oxidation by both Ce(IV) and $[Ru(bpy)_3]^{3+}$ along with extensive kinetics data are consistent with a mechanism involving rapid oxidation of polyanion **1(0)** to the **1(+4)** oxidation state and rate-limiting H_2O oxidation/O_2 evolution by **1(+4)**. Fitting of kinetics data to an integration form of the derived rate law explains the complex dependences on reactant and product concentrations.

7. Six spectroscopic, scattering, and chemical experiments indicate that the catalyst, **1(0)**, is stable in aqueous solution and under turnover conditions over the pH range involved in our catalytic studies (neutral to mildly acidic depending on buffer concentration). However, **1(0)** decomposes slowly in strong acid (pH < 1.5).

Acknowledgment. We thank the Department of Energy (grant number DE-FG02-03ER15461) for support of this research. Computer resources were provided by the Cherry Emerson Center for Scientific Computation at Emory University. We thank Dr. René Thouvenot (IPCM, Université Pierre et Marie Curie, Paris) for the acquisition of ^{29}Si and ^{183}W NMR spectra.

Supporting Information Available: Syntheses and characterization of **Rb_8K_2-1(0)**, **$[H_2N(CH_3)_2]_8K_2H_2$-Cl_4-1(0)**, and **Ce_2Cs_4-1(0)**; X-ray structure of **$[H_2N(CH_3)_2]_8K_2H_2$-Cl_4-1(0)**; details of titrations, catalytic O_2 measurements, stability studies, kinetic measurements and mechanism analysis; spectra, voltammograms of several compounds; complete ref 96. This material is available free of charge via the Internet at http://pubs.acs.org.

JA907277B

(95) Mendes, P. *Comput. Applic. Biosci.* **1997**, *9*, 563–571.
(96) Ahlrichs, R. et al. *Turbomole version 5.10, Quantum Chemistry Software*; Universität Karlsruhe, Institüt fur Physikalische Chemie und Elektrochemie, Lehrstuhl für Theoretische Chemie: Karlsruhe, 2008.
(97) Eichkorn, K.; Weigend, F.; Treutler, O.; Ahlrichs, R. *Theor. Chem. Acc.* **1997**, *97*, 119–124.
(98) Andrae, D.; Haubermann, U.; Dolg, M.; Stoll, H.; Preub, H. *Theor. Chim. Acta* **1990**, *77*, 123–141.
(99) Klamt, A.; Schüürmann, G. *J. Chem. Soc., Perkin Trans. 2* **1993**, 799–805.
(100) Baldwin, M. J.; Stemmler, T. L.; Riggs-Gelasco, P. J.; Kirk, M. L.; Penner-Hahn, J. E.; Pecoraro, V. L. *J. Am. Chem. Soc.* **1994**, *116*, 11349–11356.
(101) Dubé, C. E.; Wright, D. W.; Pal, S.; Bonitatebus, P. J.; Armstrong, W. H. *J. Am. Chem. Soc.* **1998**, *120*, 3704–3716.
(102) Rajendiran, T. M.; Kirk, M. L.; Setyawati, I. A.; Caudle, M. T.; Kampf, J. W.; Pecoraro, V. L. *Chem. Commun.* **2003**, 824–825.
(103) Mukhopadhyay, S.; Mandal, S. K.; Bhaduri, S.; Armstrong, W. H. *Chem. Rev.* **2004**, *104*, 3981–4026.
(104) Zaleski, C. M.; Depperman, E. C.; Dendrinou-Samara, C.; Alexiou, M.; Kampf, J. W.; Kessissoglou, D. P.; Kirk, M. L.; Pecoraro, V. L. *J. Am. Chem. Soc.* **2005**, *127*, 12862–12872.
(105) Pecoraro, V. L.; Hsieh, W.-Y. *Inorg. Chem.* **2008**, *47*, 1765–1778.